2024 IEEE/RSJ International Conference on Intelligent Robots and Systems (IROS)
October 14-18, 2024. Abu Dhabi, UAE

An Octopus-Inspired-Configuration Sensor Array Concept toward Torso-Oriented Magnetic Localization Task and Simulation Verification

Yichong Sun, *Graduate Student Member, IEEE*, Wai Shing Chan, Yehui Li, Heng Zhang, Yisen Huang, Haochen Hu, Philip Wai Yan Chiu, and Zheng Li, *Senior Member, IEEE*

***Abstract*— In response to torso-oriented magnetic localization tasks that require the system to have interactivity and flexibility with guaranteed accuracy, a novel bio-inspired magnetic sensor array configuration is proposed in this paper. Precisely, the ideas of the natural characteristics of octopus flexible tentacles and the "wrap" morphology are integrated into the design of the magnetic localization system based on the sensor array method. It is worth mentioning that such a design enhances the interactivity and flexibility of the localization system compared to the general planar sensor array strategy. Apart from the concept introduction, the geometry analysis of the proposed configuration is presented based on the constant curvature model. Besides, the magnetic localization algorithm for the system is presented by constructing a magnetic tracking optimization function. Eventually, the proposed concept and developed algorithm are examined in the sensor-array-simulation environment to manifest their effectiveness and applicability. The experimental results indicate that the octopus-inspired-configuration sensor array achieves a mean accuracy at a centimeter-level in our cases, and has better accuracy with a mean value of $\overline{e}$ as 0.0178 m and $\overline{SQR}_{ave}$ as 0.0883 for the center interest space compared to general planar configuration one. Moreover, the effect of the configuration error is analyzed. These results verify the feasibility and superiority of the proposed concept and hold significant practical significance in addressing the challenge associated with magnetic localization tasks toward the clinical application scenarios.**

I. INTRODUCTION

Biological systems have great potential for inspiring ideas towards the development of new technical solutions for multiple scientific fields. Specific morphologies and material features improve their adaptivity and increase their probability of survival. Up to date, inspired by living creatures, there are many robotic platforms, or mechanism systems designed with the aim of incorporating flexible characteristics [1]–[3]. These examples showcase significant morphological flexibility and interactional safety advantages over conventional articulated platforms. Apart from bio-inspired locomotion robots or mechanisms, there are also many sensing mechanisms that are designed on the basis of bio-inspired method [4], [5]. These successful cases aroused our thinking that learning from biological systems may contribute to designing a torso-oriented magnetic localization system regarding that the system requires user-friendly interactivity and adaptive flexibility with guaranteed accuracy.

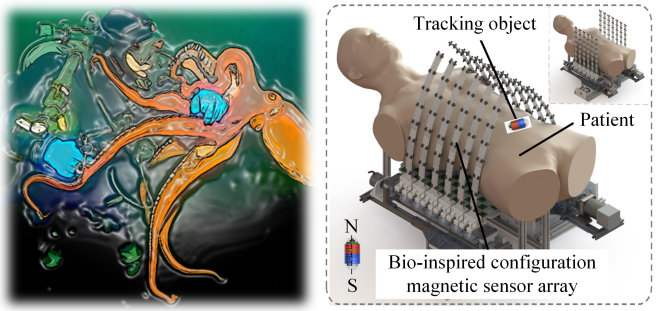

Fig. 1. Conceptual representation of octopus-inspired-configuration magnetic sensor array toward torso-oriented magnetic localization. Sensor array could "wrap" the torso like the octopus wraps around prey.

Turning to the solutions for the magnetic localization task, many remarkable efforts have been made by utilizing planar magnetic sensor array approach [6]–[8]. For example, Son *et al.* used a 2-D Hall-effect sensors array with 8×8 monoaxial Hall-effect sensors to achieve a 5-D location-ware of a dipole-modeled magnet [6]. Likewise, Xu *et al.* analyzed the selection of an optimal sensor sub-array, and achieved simultaneous magnetic actuation and location-ware [7]. Moreover, there are many sound works focusing on the magnetic localization algorithm and their applications [7], [9]–[11]. As pointed in [10], the magnetic sensor array approach is utilized with real-time and high-precision tracking for precise lung cancer radiotherapy. Besides, magnetic localization method is also applied in the gastrointestinal system [7], [9]. Admittedly, one of the wide applications of the magnetic localization approach is focusing on the localization of magnetic robots, especially for a family of magnetically actuated medical robots [12]–[15]. In terms of the medical application orientated to *in-vivo* environment, the interactivity between the human body and the localization system is a pivotal issue that needs to be considered in practice. Furthermore, from the standpoint of the magnetic sensor array technique, it has been pointed out that the measurement accuracy decreases when the magnetic tracking object moves in spaces located far

This work is supported in part by Hong Kong Research Grant Council under Projects 14203019, 14202820 and 14214322, and in part by the CUHK Strategic Seed Funding for Collaborative Research Scheme 22/21 (SSFCRS). *(Corresponding author: Zheng Li).*

Y. Sun, Y. Li, and Y. Huang are with the Department of Surgery, The Chinese University of Hong Kong, Hong Kong(e-mail: ycsun@surgery.cuhk.edu.hk; yehuili@surgery.cuhk.edu.hk; yisenhuang@surgery.cuhk.edu.hk).

H. Zhang is with the Electrical and Electronic Engineering, The University of Hong Kong, Hong Kong (e-mail: zhhku@connect.hku.hk).

W. Chan and H. Hu are with the Multi-scale Medical Robotic Center, The Chinese University of Hong Kong, Hong Kong (e-mail: waishingchan@mrc-cuhk.com; kevenhu@mrc-cuhk.com).

P. W. Y. Chiu and Z. Li are with the Department of Surgery, Chow Yuk Ho Technology Centre for Innovative Medicine, Li Ka Shing Institute of Health Science and Multi-scale Medical Robotics Center Ltd., The Chinese University of Hong Kong, Hong Kong (email: philipchiu@surgery.cuhk.edu.hk; lizheng@cuhk.edu.hk).

away from the sensor array [16]. Apparently, such a feature poses a challenge when applying the magnetic sensor array method to a scenario of *in-vivo* environment on account of the restriction of body dimension. More precisely, the planar-configuration magnetic sensor array strategy makes it hard to fit the human body as closely as possible due to the irregular body volume, leading to the measurement accuracy decrease to some extent. How to take count of both the promotion of measurement accuracy and the above-mentioned user-friendly interactivity deserves insightful investigations.

On the other note, as shown in Fig. 1-2, it can be observed that the tentacles of the octopus have high flexibility and resilience so that the octopus can adapt well to its surroundings [17]. By changing their tentacles into different kinds of curvature shapes, the octopus could well wrap around their prey or perch in habitat and breeding places to make a living. Such a "wrap" type approach embodies biological intelligence and still could inspire the design of mechanical or robotic systems in the meantime, especially in some cases where there are needs for interaction between humans and mechanical or robotic systems. Under the inspiration of such observation, the ideas of the natural characteristics of flexible tentacles and such a "wrap" strategy are integrated into the design of the magnetic sensor array configuration. On the one hand, the magnetic sensors distribute onto elastic backbones like the suckers locate on flexible tentacles. Such octopus-inspired-configuration design facilitates the bending of the backbones, further enhancing the flexibility of the sensor array. On the other hand, as illustrated in Fig. 1, these backbones form a column array with sufficient space to wrap the human body and the bending feature makes it possible that the magnetic sensors could be moved to the human body as close as possible.

Based on the above discussion, the analysis and feasibility of the proposed octopus-inspired-configuration concept will be conducted in the following. The main contributions are constructed as follows:

1) The octopus-inspired-configuration magnetic sensor array concept is proposed. To the best of authors' knowledge, such configuration concept has not been reported;
2) The theoretical methods for the geometry for the octopus-inspired-configuration sensor array, magnetic modeling for the tracking object and the magnetic localization algorithm are analyzed;
3) The feasibility of the octopus-inspired-configuration sensor-array concept is verified by the simulations and the superiority is revealed by the comparison with the planar-configuration and the analysis of the configuration error.

In the following, this article is structured as follows: Section II introduces the methodology analysis for magnetic localization of octopus-inspired-configuration sensor array. In Section III, experiments are conducted in different scenarios to demonstrate the feasibility and effectiveness of the magnetic localization approach of octopus-inspired-configuration sensor array. Finally, the conclusion and discussion are drawn in Section IV. For a better understanding for reader, standard expressions are listed as follows:

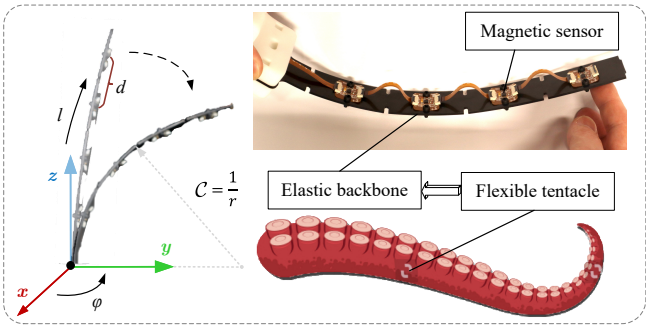

Fig. 2. Illustration of geometry modeling frame and the octopus-inspired-configuration concept for magnetic sensors.

Notations: $\mathbb{R}^n$ indicates and $\mathbb{N}$ denote n dimension Euclidean spaces and the natural number, respectively. $\mathbf{SO}(3)$ donates the 3D rotation group. Besides, the superscript "T" and subscript "$+$" stand for vector or matrix transposition and positive spaces or set.

II. Methodology Analysis

This section introduces the geometry analysis of octopus-inspired-configuration and magnetic modeling of tracking object as well as the magnetic localization algorithm.

A. Geometry of Octopus-inspired-configuration Array

Under the inspiration of the octopus tentacle, an idea has come up that the magnetic sensors are distributed along an elastic backbone which could be bent and remodelled its curvature, as illustrated in Fig. 2. Then, by setting the arrangement of many backbones, these flexible backbone could enfold a space, called measurement space for the magnetic localization. Like the octopus wraps their prey, these magnetic sensor arrays attached to these backbones "wrap" the measurement space, which is the lying place for the torso. Such octopus-inspired-configuration brings the advantage that the magnetic sensor array could be adaptive and as close to the human body as possible compared to the general planar sensor array, further enhancing the measurement accuracy.

In order to perform the magnetic localization algorithm, the configuration of the backbone should be explicit because the geometry information indicates the position of the attaching magnetic sensors, which is the base condition for the algorithm. Therefore, the reasonable assumption is given:

Assumption 1. The geometry of the backbone follows a constant curvature approximation [18], [19], when the backbone are bent in different shape, and the magnetic sensors are attached to the backbone fixedly.

With the addition of Assumption 1, the geometry parameters are defined with the backbone arc φ, curvature $\mathcal{C}$, and backbone length $l \in [0,\ Len]$, $Len \in \mathbb{R}_+$, where $\mathcal{C} = 1/r$, r defining constant radius of curvature of backbone. As shown in Fig. 2, rotating the entire elastic backbone around z-axis and x-axis by $\mathbf{R}_z(\varphi) \in \mathbf{SO}(3)$ and $\mathbf{R}_x(\theta) \in \mathbf{SO}(3)$,

respectively. The transformation from elastic backbone base to tip can be obtained as:

$$\mathbf{T} = \overbrace{\begin{bmatrix} \mathbf{R}_z(\varphi) & 0 \\ 0 & 1 \end{bmatrix}}^{\text{Rotation}} \overbrace{\begin{bmatrix} \mathbf{R}_x(\theta) & 0 \\ 0 & 1 \end{bmatrix}}^{\text{Inplane transformation}}. \tag{1}$$

The equation (1) can be written in terms of geometry parameters $(\varphi, \mathcal{C}, l)$ by

$$\mathbf{T}(\varphi,\mathcal{C},l) = \left[\begin{array}{cc|c} \multicolumn{2}{c|}{\mathbf{T}_{11}} & \mathbf{T}_{12} \\ \hline -\cos\varphi\sin\mathcal{C}l & -\sin\varphi\sin\mathcal{C}l & \cos\mathcal{C}l \quad \frac{\sin\mathcal{C}l}{\mathcal{C}} \\ 0 & 0 & 0 \quad 1 \end{array}\right] \tag{2}$$

with the followings

$$\mathbf{T}_{11} = \left[\begin{array}{c|c} \cos^2\varphi(\cos\mathcal{C}l-1)+1 & \cos(\varphi)\sin(\varphi)(\cos\mathcal{C}l-1) \\ \cos\varphi\sin\varphi(\cos\mathcal{C}l-1) & \cos^2\varphi\,(1-\cos\mathcal{C}l)+\cos\mathcal{C}l \end{array}\right]$$

$$\mathbf{T}_{12} = \begin{bmatrix} \sin\mathcal{C}l\cos\varphi & \frac{\cos\varphi(1-\cos\mathcal{C}l)}{\mathcal{C}} \\ \sin\mathcal{C}l\sin\varphi & \frac{\sin\varphi(1-\cos\mathcal{C}l)}{\mathcal{C}} \end{bmatrix}$$

where $\mathbf{T}(\varphi,\mathcal{C},l)$ represents transformation at any length point l with curvature $\mathcal{C}$ and arc φ.

In order to acquire the position of each sensor, these backbones are divided into left-array m backbones and right array $m \in \mathbb{N}_+$ backbones with a separation distance $D \in \mathbb{R}_+$ and the distance between every adjacent backbone is $d \in \mathbb{R}_+$ in x-axis. An assumption is provided that the left-array (L) has an unified backbone curvature $\mathcal{C}^L$ while the right-array (R) has an unified backbone curvature $\mathcal{C}^R$. Given that there are $n \in \mathbb{N}_+$ magnetic sensors distributed in the backbone length set $\mathcal{L} \triangleq \{l_1, l_2, ..., l_n\}$. The position of n magnetic sensor in m can be given by

$$\begin{cases} \begin{bmatrix} \mathbf{P}^L_{(m,n)} & 1 \end{bmatrix}^\intercal = \mathbf{T}(\varphi,\mathcal{C}^L,l_n) * \mathbf{I}_{tran} + \mathbf{D}_L(m) \\ \begin{bmatrix} \mathbf{P}^R_{(m,n)} & 1 \end{bmatrix}^\intercal = \mathbf{T}(\varphi,\mathcal{C}^R,l_n) * \mathbf{I}_{tran} + \mathbf{D}_R(m) \end{cases} \tag{3}$$

with the followings

$$\begin{aligned} \mathbf{D}_L(m) &= \begin{bmatrix} 0 & m*d & 0 & 0 \end{bmatrix}^\intercal \\ \mathbf{D}_R(m) &= \begin{bmatrix} D & m*d+\frac{d}{2} & 0 & 0 \end{bmatrix}^\intercal \\ \mathbf{I}_{tran} &= \begin{bmatrix} 0 & 0 & 0 & 1 \end{bmatrix}^\intercal \end{aligned}$$

where $\mathbf{P}_{(m,n)}$ is a position vector indicates the position of (m,n) magnetic sensor in the same frame and $\mathbf{D}_{(\cdot)}(m)$ and $\mathbf{I}_{tran}$ represents offset and transformation vector, severally. Up to here, the method to obtain the geometry of the backbone and the positions of sensors has been presented, based on which the localization algorithm could be developed. Before that, the magnetic modeling of the tracking object should be analyzed, which will be discussed next.

B. Magnetic Modeling of Tracking Object

As for the tracking magnetic object inside the inner-torso, it is defined as medical robots which are embedded with magnets, for example magnetically-actuated capsule endoscope, magnetically-actuated colonoscope and so on [13], [20], [21]. In the paper, it is assumed that the magnets embedded in the tracking object could be modelled as a dipole magnet [22], such that the magnetic field can be represented as:

$$\begin{aligned} \mathbf{B}\left(\mathbf{P}^{(\cdot)}_{(m,n)}, \mathbf{P}_o, \mathbf{m}\right) = \frac{\mu_0}{4\pi\left\|\mathbf{r}^o_{(m,n)}\right\|^5}\Big(3\mathbf{r}^o_{(m,n)}\left(\mathbf{r}^o_{(m,n)}\right)^\intercal \\ - \left\|\mathbf{r}^o_{(m,n)}\right\|^2 \mathbf{I}_{3\times3}\Big)\,\mathbf{m} \end{aligned} \tag{4}$$

with the followings

$$\mathbf{r}^o_{(m,n)} = \mathbf{P}_o - \mathbf{P}^{(\cdot)}_{(m,n)}$$

where $\mu_0 = 4\pi \times 10^7\ \mathrm{T\cdot m\cdot A^{-1}}$ is the permeability of free space, and $\mathbf{P}_o \in \mathbb{R}^3$ is the position vector of the tracking object and $\mathbf{m} \in \mathbb{R}^3$ is the magnetic dipole moment. $\mathbf{B}\left(\mathbf{P}^{(\cdot)}_{(m,n)}, \mathbf{P}_o, \mathbf{m}\right)$ is the magnetic field generated by the tracking object while the real magnetic field measured by the magnetic sensor array could be different because there are noise errors existing ($(\cdot)$ defines L or R). Hence, for the conduction of the later simulation test, the perhaps is given as follows.

Assumption 2. The magnetic field measured by (m,n) magnetic sensor consist of the real value $\mathbf{B}\left(\mathbf{P}^{(\cdot)}_{(m,n)}, \mathbf{P}_o, \mathbf{m}\right)$ and the sensor noise $\mathbf{B}_{noi} = \begin{bmatrix} B^x_{noi}(\cdot) & B^y_{noi}(\cdot) & B^z_{noi}(\cdot) \end{bmatrix}^\intercal$ and each vector component obeys the distribution [23], [24]:

$$B^*_{noi}(v) \sim \frac{1}{\sigma\sqrt{2\pi}}\exp\left(-\frac{(v-\mu)^2}{2\sigma^2}\right), * \text{ is } x, y, \text{or } z$$

where σ is the mean of distribution and μ is the standard deviation.

Under the introduction of Assumption 2, the measurement magnetic field received by (m,n) magnetic sensor could be given by:

$$\mathbf{B}_t\left(\mathbf{P}^{(\cdot)}_{(m,n)}, \mathbf{P}_o, \mathbf{m}\right) = \mathbf{B}\left(\mathbf{P}^{(\cdot)}_{(m,n)}, \mathbf{P}_o, \mathbf{m}\right) + \bar{N}\mathbf{B}_{noi} \tag{5}$$

where $\bar{N} \in \mathbb{R}_+$ is the amplification coefficient for the sensor noise vector $\mathbf{B}_{noi}$. Afterwards, the magnetic localization algorithm based on the analyzed model and geometry information can be inferred next.

C. Magnetic Localization Algorithm and Analysis

The developed magnetic tracking algorithm solves the optimal $\mathbf{P}_o$ by the virtual of minimizing a cost function using Levenberg-Marquardt method [25]. The cost function for magnetic tracking is constructed as:

$$\begin{aligned} C = \sum_{i=1}^{m}\sum_{j=1}^{n}\Big(&\mathbf{B}\left(\mathbf{P}^L_{(i,j)}, \mathbf{P}_o, \mathbf{m}\right) + \mathbf{B}\left(\mathbf{P}^R_{(i,j)}, \mathbf{P}_o, \mathbf{m}\right) \\ &-\mathbf{B}_t\left(\mathbf{P}^L_{(i,j)}, \mathbf{P}_o, \mathbf{m}\right) - \mathbf{B}_t\left(\mathbf{P}^R_{(i,j)}, \mathbf{P}_o, \mathbf{m}\right)\Big). \end{aligned}$$

Then, the magnetic tracking algorithm can be performed by solving the following optimization function

$$\begin{aligned} \tilde{\mathbf{P}}_o &= \arg\min_{\mathbf{P}_o}\|C\| \\ \text{s.t. } \mathbf{m} &= \mathbf{m}_o,\ \sigma = \sigma_c,\ \mu = \mu_c \end{aligned} \tag{6}$$

where $\mathbf{m}_o,\ \sigma_c,\ \mu_c$ are known conditions. By solving (6), the tracking position $\tilde{\mathbf{P}}_o$ is obtained. On the other note,

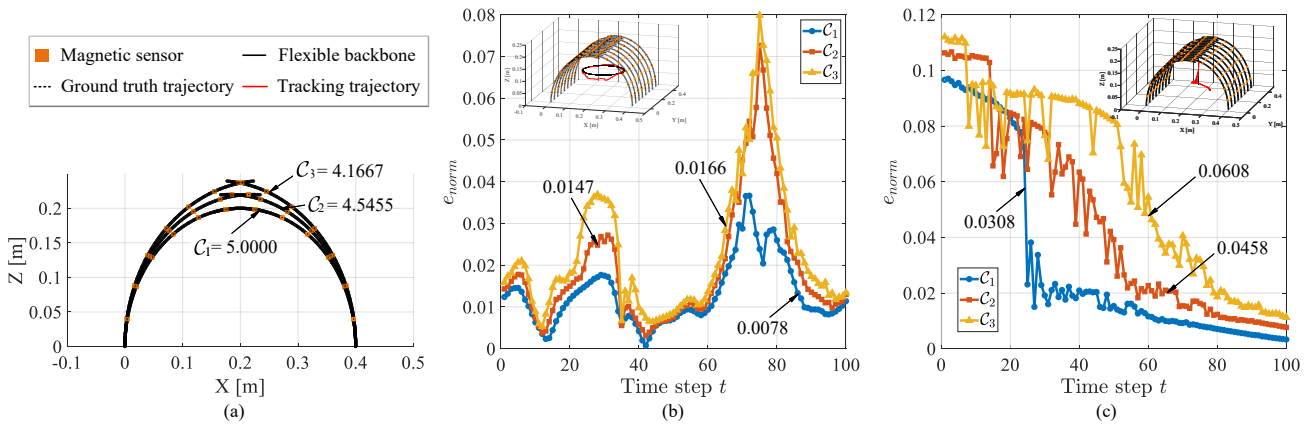

Fig. 3. Experimental results of arc and line tracking cases under different curvature octopus-inspired-configuration sensor array. (a) Illustration of different curvature backbones sensor array and legends. (b) e_{norm} and $\bar{e}$ results for three arc tracking tests. (c) e_{norm} and $\bar{e}$ results for three line tracking tests. (Sub-figures in (b) and (c) show the octopus-inspired-configuration sensor array, ground truth trajectory and algorithm tracking results and the indication of numbers with arrows is the mean value of referencing data.)

a significant parameter, *Signal Quality Ratio* (SQR) [6], is defined to evaluate the relationship between the magnetic field and the measured one which consists of other magnetic field error terms. In the context, the average SQR for our case is introduced and formed as

$$\overline{\mathrm{SQR}} = \log_{10}\left(1 + \frac{1}{mn}\sum_{i=1}^{m}\sum_{j=1}^{n}\frac{\left\|\mathbf{B}\left(\mathbf{P}_{(i,j)}^{(\cdot)}, \mathbf{P}_o, \mathbf{m}\right)\right\|}{\left\|\mathbf{B}_t\left(\mathbf{P}_{(i,j)}, \mathbf{P}_o, \mathbf{m}\right)\right\|}\right)$$

which generates

$$\overline{\mathrm{SQR}} \propto \log_{10}\left(1 + \frac{1}{mn}\sum_{i=1}^{m}\sum_{j=1}^{n}\left(1 + \left\|\frac{c_{noi}}{\mathbf{r}_{(m,n)}^{o}}\right\|\right)^{3}\right) \quad (7)$$

where c_{noi} is constant parameter defined by sensor noise term $\bar{N}\mathbf{B}_{noi}$.

Remark. From the relation (7), it can be found that if the sum of $\mathbf{r}_{(m,n)}^{o}$ increases, $\overline{\mathrm{SQR}}$ turns to bigger. This is the reason why proposing octopus-inspired-configuration sensor array for the torso-oriented magnetic localization application. Compared to the existing planar sensor array, the proposed approach could change the position of magnetic sensors, chasing magnetic sensors to be as close to the torso as possible. In consequence, a higher level of $\overline{\mathrm{SQR}}$ is guaranteed. Such a flexible configuration also has superiority in applicability toward the interaction between the magnetic sensor array and the human body.

III. Simulation Validation

In this section, the effectiveness and superiority of the proposed concept and approach are demonstrated by conducting simulation experiments. First, the tracking accuracy is evaluated by:

$$e_{norm}(T) = \|\tilde{\mathbf{P}}_o - \mathbf{P}_{\mathcal{G}}(T)\|,\ \bar{e} = \frac{1}{N}\sum_{T=0}^{N} e_{norm}(T)$$

where $e_{norm}(T)$ and $\bar{e}$ are the norm of the position error at sampling time T and the mean of all position error, respectively, and $\mathbf{P}_{\mathcal{G}} = [x_{\mathcal{G}},\ y_{\mathcal{G}},\ z_{\mathcal{G}}] \in \mathbb{R}^3$ is ground truth.

TABLE I

Setup Parameters of Magnetic Sensor Array

Parameters	m	n	d	D	$\mathcal{L}$
Values	8	7	0.06 [m]	0.4 [m]	{0.06, ..., 0.42} [m]

A. Verification of Octopus-inspired-configuration Concept

First, the arc and line tracking experiments are conducted. The setup parameters of the octopus-inspired-configuration are given in Tab. I. Then, two sets of the ground truth position $\mathbf{P}_{\mathcal{G}}^{arc}$ and $\mathbf{P}_{\mathcal{G}}^{line}$ of the tracking magnet are set as

$$\mathbf{P}_{\mathcal{G}}^{arc}\begin{cases} x_{\mathcal{G}}(T) = 0.1\cos(2\pi/100T) + 0.2, \\ y_{\mathcal{G}}(T) = 0.1\sin(2\pi/100T) + 0.225, z_{\mathcal{G}}(T) = 0.1, \end{cases}$$

$$\mathbf{P}_{\mathcal{G}}^{line}\begin{cases} x_{\mathcal{G}}(T) = 0.2, y_{\mathcal{G}} = 0.225, z_{\mathcal{G}}(T) = \frac{T}{1000} + 0.005, \end{cases}$$

with time step $T \in \mathbb{N}_{[0,\ 100]}$. Setting magnetic moment $\mathbf{m}_o$ of the tracking magnet as $[0\ 0\ 2]^{\intercal}$ A $\cdot$ m^2 and conditions $\sigma_c = 2,\ \mu_c = 0,\ \bar{N} = 1$ Gs (high signal noise coefficient is set to manifest differences in different sensor array layouts). Besides, in order to test the feasibility of octopus-inspired-configuration sensor array with different curvatures, three are sets of sensor array with curvatures $\mathcal{C}^L \in \{\mathcal{C}_1, \mathcal{C}_2, \mathcal{C}_3\}$ and $\mathcal{C}^R = -\mathcal{C}^L$. With the aid of (3)-(6), the tests are conducted and the e_{norm} results are shown in Fig. 3, which indicate that the $\bar{e}$ for $\mathcal{C}_1, \mathcal{C}_2$, and $\mathcal{C}_3$ arc cases are 0.0078, 0.0147, 0.0166 m, separately, and for line cases are 0.0308, 0.0458, 0.0608 m, severally.

From the analysis of these results, it is straightforward that the concept of an octopus-inspired-configuration sensor array could perform magnetic localization and achieve a mean accuracy at a centimeter level in such experimental setup. Moreover, the bigger the curvature, the better localization accuracy, which satisfies the rule that pursuing the compact measured space within the same sensor array will enhance the mean measurement accuracy as discussed in Section II.

B. Superiority when Compared to Planar Configuration

This test analyses the measurement space accuracy by comparing octopus-inspired and planar configurations. In the

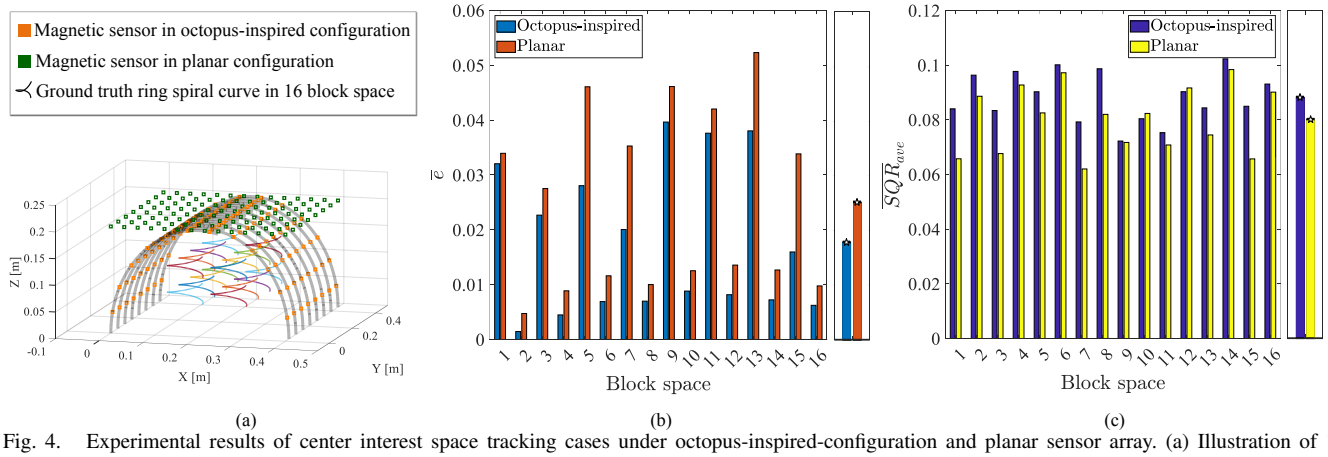

(a) (b) (c)

Fig. 4. Experimental results of center interest space tracking cases under octopus-inspired-configuration and planar sensor array. (a) Illustration of 16 rising spiral curves in center interest space blocks and legends. (b) $\overline{e}$ results for 16 rising spiral curves tracking tests by octopus-inspired-configuration and planar sensor array. (c) $\overline{SQR}_{ave}$ results for 16 rising spiral curves tests by octopus-inspired-configuration and planar sensor array. (Right-side sub-figures inside (b) and (c) show mean value of all $\overline{e}$ and $\overline{SQR}_{ave}$ for 16 cases with "$\star$" tag.)

real applications toward the torso-inner, the interest space is mainly in the center, which is still the most challenging space to achieve accurate localization because the measurement accuracy will decrease when the tracking object goes to the space located far away from the sensors [16].

The interest space is divided into 16 blocks of space, and in each block space, there are rising spiral curves set as the ground truth for further conducting magnetic localization, shown in Fig. 4 (a). Each curve $\mathbf{P}_{\mathcal{G}}^{rs}$ is set as

$$\mathbf{P}_{\mathcal{G}}^{rs}\begin{cases} x_{\mathcal{G}}(T) = 0.04\cos(2\pi/100T), \\ y_{\mathcal{G}}(T) = 0.04\sin(2\pi/100T), z_{\mathcal{G}}(T) = 0.0004T. \end{cases}$$

Then, by setting $\mathcal{C}^L = \mathcal{C}_1$ and $\mathcal{C}^R = -\mathcal{C}^L$ and other conditions as the same with the test in subsection A, and designing a planar sensor array with 14×8 magnetic sensors distributing uniformly and covering the same projection area as the octopus-inspired-configuration sensor array, the simulations are conducted and the results are indicated in Fig. 4 with performances $\overline{e}$ and $\overline{SQR}_{ave} = \frac{1}{N}\sum_{T=0}^{N}\overline{SQR}(T)$.

Results show that the mean value of $\overline{e}$ for octopus-inspired-configuration is 0.0178 m, compared with 0.0251 m for planar configuration, and the mean value of $\overline{SQR}_{ave}$ for octopus-inspired and planar configuration are 0.0883 and 0.0802, respectively. From the analysis of these data, it can be concluded that for the center interest space, the proposed octopus-inspired-configuration sensor array has a better mean value of $\overline{e}$, and a higher mean value of $\overline{SQR}_{ave}$, which show the superiority in measurement accuracy.

C. Analysis of Configuration Error

As is well-known, the geometry of elastic backbone is difficult to measure in the real world even though the constant curvature approximation in Assumption 1 could represent the geometry to a great extent. The configuration errors exist inevitably in practice due to the limitation of sensing or the approximation assumption. In response to this concern, the measurement accuracy error generated by the configuration errors is analyzed in this subsection by introducing the uncertain configuration errors in the algorithm.

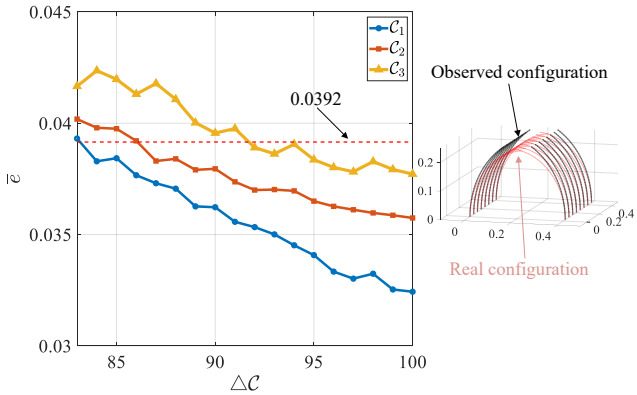

Fig. 5. Experimental results of arc tracking tests under different configuration errors. (Right-side figure illustrates configuration error.)

Likely, setting conditions as the same as the test in subsection A, and the ground truth position $\mathbf{P}_{\mathcal{G}}^{c}$ is given by

$$\mathbf{P}_{\mathcal{G}}^{arc}\begin{cases} x_{\mathcal{G}}(T) = 0.1\cos(2\pi/100T) + 0.2, \\ y_{\mathcal{G}}(T) = 0.1\sin(2\pi/100T) + 0.225, z_{\mathcal{G}}(T) = 0.09. \end{cases}$$

Next, here defines $\mathcal{C}_{observe} = \triangle\mathcal{C}/100\ \mathcal{C}_{real}$, which means that the observed curvature is smaller than real one and there exists an error, illustrated in Fig. 5. By conducting the algorithm for $\mathcal{C}_{real} \in \{\mathcal{C}_1, \mathcal{C}_2, \mathcal{C}_3\}$, the $\overline{e}$ results for these three cases are obtained, shown in Fig. 5. Obviously, it can be seen that when $\triangle\mathcal{C}$ decreases, the $\overline{e}$ for all cases increase.

Moreover, $\overline{e}$ for the planar configuration under the same experimental conditions is calculated and shown in Fig. 5 with the red-dot line. For the $\mathcal{C}_1$ case, the superiority of the octopus-inspired method will disappear when $\triangle\mathcal{C}$ comes to 80. The same for $\mathcal{C}_2$ and $\mathcal{C}_3$ cases when according $\triangle\mathcal{C}$ are about 86 and 94, respectively. Such results reveal that it is necessary to figure out the accurate configuration of these backbones because, essentially the accurate pose of magnetic sensors places a pivotal base for the conduction of the algorithm, affecting the final localization accuracy.

IV. Discussion and Conclusion

The article has presented a novel octopus-inspired-configuration magnetic sensor array solution with the aim

of fulfilling torso-oriented localization tasks for magnetic robots in clinical scenarios. At first, the concept of octopus-inspired-configuration sensor array was proposed by means of imitating the octopus's flexible tentacle structure and its wrap morphology. Then, a constant curvature approximation method was applied to model the geometry of the octopus-inspired-configuration, further obtaining all positions of magnetic sensors. Next, the tracking magnetic robot was assumed as a dipole magnetic source, whose magnetic field model was presented for the construction of the magnetic localization algorithm. The algorithm was operated by virtual of the minimizing of a cost function. At last, the magnetic localization performance was manifested on a magnetic sensor-array-simulation. The feasibility and superiority of the proposed concept were verified by a set of experiments and comparisons with general planar cases.

Albeit the proposed concept successfully performs the magnetic localization in sensor-array-simulation, there are certain issues deserving more profound research: (i) Given that the focus of this work is concept verification, all tests are conducted in the magnetic sensor-array-simulation. The real-world prototype should be constructed. (ii) Due to the fact that the aim of this solution is for the torso-oriented environment, whereupon, evaluating the performance of the proposed approach in animals and humans is needed. (iii) Assumption 1 in this paper could be ideal to some degree. That's also the reason why the analysis of configuration errors is performed in the simulation validation. Based on the tests, it can be found that the exact configuration of these backbones is of the utmost importance because, in essence, the precise position of magnetic sensors acts as a fulcrum for the execution of the algorithm, affecting the final precision of magnetic localization. In practice, techniques like precise modeling approach [26] or configuration calibration should be taken into account [27]. All these issues and considerations derive the motivations for our future work.

REFERENCES

[1] R. Pfeifer, M. Lungarella, and F. Iida, "Self-organization, embodiment, and biologically inspired robotics," *Science*, vol. 318, no. 5853, pp. 1088–1093, 2007.

[2] G. Yan, H.-X. Zou, S. Wang, L.-C. Zhao, Z.-Y. Wu, and W.-M. Zhang, "Bio-inspired vibration isolation: Methodology and design," *Appl. Mech. Rev.*, vol. 73, no. 2, p. 020801, 2021.

[3] S. T. Frey, A. T. Haque, R. Tutika, E. V. Krotz, C. Lee, C. B. Haverkamp, E. J. Markvicka, and M. D. Bartlett, "Octopus-inspired adhesive skins for intelligent and rapidly switchable underwater adhesion," *Sci. Adv.*, vol. 8, no. 28, p. eabq1905, 2022.

[4] F. A. Hassani, "Bioreceptor-inspired soft sensor arrays: recent progress towards advancing digital healthcare," *Soft Science*, vol. 3, no. 4, pp. 1–33, 2023.

[5] Q. Xin, J. Zhang, Z. Han, H. Zhao, T. Hou, Y. Liu, S. Niu, Q. Han, Z. Mu, B. Li, *et al.*, "Advanced bio-inspired mechanical sensing technology: Learning from nature but going beyond nature," *Adv. Mater. Technol.*, vol. 8, no. 1, p. 2200756, 2023.

[6] D. Son, S. Yim, and M. Sitti, "A 5-D localization method for a magnetically manipulated untethered robot using a 2-D array of hall-effect sensors," *IEEE/ASME Trans. Mechatron.*, vol. 21, no. 2, pp. 708–716, 2016.

[7] Y. Xu, K. Li, Z. Zhao, and M. Q.-H. Meng, "Adaptive simultaneous magnetic actuation and localization for WCE in a tubular environment," *IEEE Trans. Robot.*, vol. 38, no. 5, pp. 2812–2826, 2022.

[8] M. Zhang, L. Yang, C. Zhang, Z. Yang, and L. Zhang, "A 5-D large-workspace magnetic localization and actuation system based on an eye-in-hand magnetic sensor array and mobile coils," *IEEE Trans. Instrum. Meas.*, vol. 72, pp. 1–11, 2023.

[9] S. Su, S. Yuan, M. Xu, H. Gao, X. Yang, and H. Ren, "AMagPoseNet: Real-time 6-DoF magnet pose estimation by dual-domain few-shot learning from prior model," *IEEE Trans. Ind. Inform.*, 2023.

[10] H. Dai, L. Dong, B. Lv, Y. Chen, S. Song, and S. Su, "Feasibility study of permanent magnet-based tumor tracking technique for precise lung cancer radiotherapy," *IEEE Trans. Instrum. Meas.*, vol. 70, pp. 1–10, 2020.

[11] Y. Xu, K. Li, Z. Zhao, and M. Q.-H. Meng, "Evaluation of different control strategies for trajectory following of a robotic capsule endoscope under rotating magnetic actuation," *IEEE Trans. Autom. Sci. Eng.*, 2022.

[12] Y. Sun, Y. Li, J. Li, W. Y. Ng, Y. Xian, Y. Huang, P. W. Y. Chiu, and Z. Li, "Model-based bending control of magnetically-actuated robotic endoscopes for automatic retroflexion in confined spaces," in *2023 IEEE/RSJ International Conference on Intelligent Robots and Systems (IROS)*, pp. 8439–8445, IEEE, 2023.

[13] A. Z. Taddese, P. R. Slawinski, M. Pirotta, E. De Momi, K. L. Obstein, and P. Valdastri, "Enhanced real-time pose estimation for closed-loop robotic manipulation of magnetically actuated capsule endoscopes," *Int. J. Rob. Res.*, vol. 37, no. 8, pp. 890–911, 2018.

[14] Z. Cui, J. Li, W. Li, T. Cheng, P. W. Y. Chiu, and Z. Li, "Online dual neural network receding-horizon tracking control for magnetic actuated endoscopic robots," *IEEE/ASME Trans. Mechatron.*, 2023.

[15] X. Yu, J. Wang, J. Su, and S. Song, "Inchworm-like biomimetic magnetic-driven robotic shell for capsule endoscope in a tubular environment," *IEEE/ASME Trans. Mechatron.*, 2024.

[16] H. Zhang, Y. Li, and Z. Li, "6-D spatial localization of wireless magnetically actuated capsule endoscopes based on the fusion of hall sensor array and imu," *IEEE Sens. J.*, vol. 22, no. 13, pp. 13424–13433, 2022.

[17] B. Mazzolai, L. Margheri, M. Cianchetti, P. Dario, and C. Laschi, "Soft-robotic arm inspired by the octopus: Ii. from artificial requirements to innovative technological solutions," *Bioinspiration Biomim.*, vol. 7, no. 2, p. 025005, 2012.

[18] M. Rolf and J. J. Steil, "Constant curvature continuum kinematics as fast approximate model for the bionic handling assistant," in *2012 IEEE/RSJ International Conference on Intelligent Robots and Systems*, pp. 3440–3446, IEEE, 2012.

[19] R. J. Webster III and B. A. Jones, "Design and kinematic modeling of constant curvature continuum robots: A review," *Int. J. Rob. Res.*, vol. 29, no. 13, pp. 1661–1683, 2010.

[20] Y. Li, W. Y. Ng, W. Li, Y. Huang, H. Zhang, Y. Xian, J. Li, Y. Sun, P. W. Y. Chiu, and Z. Li, "Towards semi-autonomous colon screening using an electromagnetically actuated soft-tethered colonoscope based on visual servo control," *IEEE. Trans. Biomed. Eng.*, 2023.

[21] D. Ye, J. Xue, S. Yuan, F. Zhang, S. Song, J. Wang, and M. Q.-H. Meng, "Design and control of a magnetically-actuated capsule robot with biopsy function," *IEEE. Trans. Biomed. Eng.*, vol. 69, no. 9, pp. 2905–2915, 2022.

[22] J. J. Abbott, E. Diller, and A. J. Petruska, "Magnetic methods in robotics," *Annu. Rev. Control Robot. Auton. Syst.*, vol. 3, pp. 57–90, 2020.

[23] J. K. Patel and C. B. Read, *Handbook of the normal distribution*, vol. 150. CRC Press, 1996.

[24] Y. Hu, G. Chen, Z. Li, and A. Knoll, "Robot policy improvement with natural evolution strategies for stable nonlinear dynamical system," *IEEE Trans. Cybern.*, vol. 53, no. 6, pp. 4002–4014, 2022.

[25] N. Yamashita and M. Fukushima, "On the rate of convergence of the levenberg-marquardt method," in *Topics in Numerical Analysis: With Special Emphasis on Nonlinear Problems*, pp. 239–249, Springer, 2001.

[26] H. Cheng, H. Liu, X. Wang, and B. Liang, "Approximate piecewise constant curvature equivalent model and their application to continuum robot configuration estimation," in *2020 IEEE International Conference on Systems, Man, and Cybernetics (SMC)*, pp. 1929–1936, IEEE, 2020.

[27] D. Son, X. Dong, and M. Sitti, "A simultaneous calibration method for magnetic robot localization and actuation systems," *IEEE Trans. Robot.*, vol. 35, no. 2, pp. 343–352, 2018.